Enhancements of extreme ultraviolet emission using prepulsed Sn laser-produced plasmas for advanced lithography applications

J. R. Freeman, S. S. Harilal,[a] and A. Hassanein
Center for Materials Under Extreme Environment, School of Nuclear Engineering, Purdue University, West Lafayette, Indiana 47907, USA

(Received 31 July 2011; accepted 1 September 2011; published online 18 October 2011)

Laser-produced plasmas (LPP) from Sn targets are seriously considered to be the light source for extreme ultraviolet (EUV) next generation lithography, and optimization of such a source will lead to improved efficiency and reduced cost of ownership of the entire lithography system. We investigated the role of reheating a prepulsed plasma and its effect on EUV conversion efficiency (CE). A 6 ns, 1.06 μm Nd:yttrium aluminum garnet laser was used to generate the initial plasma that was then reheated by a 40 ns, 10.6 μm CO_2 laser to generate enhanced EUV emission from a planar Sn target. The effects of prepulsed laser intensity and delay timings between the prepulsed and the pumping pulse were investigated to find the optimal pre-plasma conditions before the pumping pulse. The initial optimization of these parameters resulted in 25% increase in CE from the tin LPP. The cause of increased EUV emission was identified from EUV emission spectra and ion signal data. © *2011 American Institute of Physics*. [doi:10.1063/1.3647779]

I. INTRODUCTION

Extreme ultraviolet lithography is being considered as the light source for the next generation of semiconductor manufacturing. In order for EUV lithography to become commercially viable, an efficient and clean EUV source emitting at 13.5 nm must be identified. The 13.5 nm was chosen as the wavelength because multilayer mirrors made of Mo/Si provide relatively high reflectivity of about 70% at this wavelength and do not pose health risks of Be-based multilayer mirrors at other EUV wavelengths. The Mo/Si mirrors also exhibit a broader reflectivity peak than Be-based mirrors, allowing for a larger bandwidth interval ($\pm$ 2%) for 13.5 nm radiation collection.[1] However, high volume manufacturing (HVM) tools will require[2] in-band EUV power around 200 W, with future systems requiring up to 500 W, which is considered to be very challenging. An efficient and debris-free source is the prerequisite for moving lithography technology from optical to EUV wavelengths.

Once a wavelength was identified for EUV lithography, a source needed to be identified. The two competing methods currently considered for generating EUV photons are the discharge-produced plasma (DPP) and laser-produced plasma (LPP). Considerable efforts for improving the efficiencies of both techniques are ongoing.[2–4] The EUV emission of several materials was investigated, and it was found that Li, Xe, and Sn plasmas emit well within the 13.5 nm bandwidth. Li is a line emitter while Xe and Sn exhibit broad-band emission, all centered near 13.5 nm.[5] Radiation near 13.5 nm from Xe plasmas comes only from the transition by Xe^{10+} ions, while other transitions emit strongly near 11 nm, which is not useable. For Xe DPP systems, conversion efficiency (CE) of only about 1% has been achieved.[6] Using several experimental schemes, Xe LPP systems have only been able to achieve a CE of 0.6%−1.0%.[6–8] Emission from Sn plasmas is broad and peaks at 13.5 nm. This region is referred to as the Sn unresolved transition array (UTA) and is caused by transitions in Sn^{8+} to Sn^{13+} ions. Due to its high CE of 13.5 nm in-band radiation, Sn has become the main current material of interest for EUV lithography. Using a laser pulse to vaporize[9] the target before discharge, Sn DPP systems have achieved CE of about 2%. One limitation for DPP systems is a source size larger than the lithography system's etendue allows. For LPP, the source size is smaller and etendue mismatch is not a concern. Sn LPP research[3,10,11] has yielded higher experimental CE results of 2%−5% depending on experimental parameters, with modeling studies predicting up to 7%.[12] Due to better scalability for HVM scanners, LPP research has taken precedent over DPP efforts for future high-power EUV sources.[2,13]

In a LPP system, several key systems specifications must be chosen which will affect the EUV emitting plasma and the cleanness of the system. These include target geometry, laser parameters, laser irradiation scheme, and debris mitigation techniques.[5,14] For generating Sn plasmas, several target geometries have been explored, including thin film,[15] planar slab,[16] grooved planar slab,[11] Sn-doped foam,[17] and microdroplet.[12,18,19] Grooved planar Sn targets have been shown to achieve CE of 5% because the grooves cause hydrodynamic confinement of the plasma, generating an area of efficient EUV production.[11] Thin films, Sn-doped materials, and microdroplets are used as mass-limited targets. Sn LPPs generate significant amounts of debris that over time cover and degrade the collection optics of HVM systems, thereby limiting the lifetime of the system. Using mass-limited targets, the EUV emitting plasma will be less dense, and less debris will be collected on the optics. While mass-limited targets will emit fewer EUV photons due to a lower plasma density, the lower photon count is offset by less self-absorption because of lower plasma opacity.[20] For this reason mass-limited targets are able to provide similar CE to larger-mass targets. Laser

[a]Electronic mail: sharilal@purdue.edu.

parameters such as wavelength,[10] intensity,[21] and spot size[22] have been shown to affect the CE of EUV and the ion/debris dynamics of Sn plasmas.

One of the most crucial parameters for optimizing CE from LPPs is the laser wavelength used to induce emission. Initial LPP EUV research was conducted primarily with Nd:YAG lasers operating at 1.06 μm. In 2005, Tanaka *et al.*[23] showed the potential of the CO_2 laser at 10.6 μm as EUV sources. A CO_2 LPP provides better spectral purity compared to Nd:YAG LPP due to lower plasma opacity.[10] Though a CO_2 laser produces ions with higher kinetic energies than those from Nd:YAG laser, the particle emission and debris accumulation from CO_2 LPP was less than one fourth that from Nd:YAG laser when compared at the same laser energy.[16,24,25] The difference between CO_2 and Nd:YAG LPPs is due to their large difference in critical densities. Note[10] that critical density is inversely proportional to the laser wavelength: $n_{ec} \propto \lambda^{-2}$. When the plasma density is higher than the critical density for the CO_2 LPP, the plasma is considered opaque to further laser irradiation. Because of this, the CO_2 laser radiation is absorbed in the outer region of the plasma, rather than penetrating through the plasma and heating/ablating more material from the target surface. This causes higher ion energies and less ablated target material, leading to significantly lower particle emission. Due to its shorter wavelength, the opposite is often true for Nd:YAG laser radiation. When plasma density is lower than the critical density, the Nd:YAG radiation is able to penetrate through the plasma, depositing more energy near to the critical density region, rather than reheating the already ablated material. This generates lower ion energies, but higher particle emission due to the increase in ablated target material.

Implementation of a double pulse laser irradiation scheme has also been shown to increase EUV and x-ray yield by other researchers.[4,18,26,27] Recent modeling studies showed that such a scheme will provide CE $\sim 7\%$.[13] In a double pulse scheme, parameters of each laser pulse must be optimized to achieve the best results, greatly increasing the number of variables to consider for optimizing the CE. Ideally, in a double pulse scheme, a lower energy pre-pulse will ablate the target of interest, and the second pulse will be used to reheat the plasma efficiently to emit more EUV photons. In this article, we investigated the effect on EUV conversion efficiency of a CO_2 laser reheating a plasma, initially generated by Nd:YAG prepulse. The prepulse laser intensity and the delay timings between the prepulse and pumping pulse were varied to determine the optimum conditions for enhancing the CE. The EUV emission spectra and ion yield data from a Faraday cup (FC) were used to identify the direct causes of CE enhancements that were seen.

II. EXPERIMENTAL DETAILS

A schematic illustration of the experimental setup in our center for materials under extreme environment (CMUXE) lab is shown Fig. 1. Two lasers were used in our experiments. A 6 ns full width half maximum (FWHM), 1.06 μm Nd:YAG laser was used as the prepulse to generate a pre-plasma serving as a lower-density Sn target, and a 40 ns FWHM, 10.6 μm transversely excited atmospheric (TEA) CO_2 laser was used as the pumping pulse to reheat the pre-plasma and generate EUV emission. A plasma shutter was used with the CO_2 laser to eliminate the long tail of the laser pulse, resulting in a Gaussian pulse profile that interacts with the target.[28] A planar Sn target was positioned in the center of a vacuum chamber of pressure $\sim 5 \times 10^{-6}$ Torr. Both lasers interacted with the target at an angle of $\sim 5^\circ$ off-normal. The target was moved to a fresh position for each laser shot. Spot sizes used were ~ 225 μm for the CO_2 laser and 100 μm and 250 μm for the Nd:YAG laser. A combination of two delay generators (DG) was used to change the timing between pulses from the two lasers. One DG was used to trigger the flash lamps of the Nd:YAG laser at 10 Hz in order to minimize thermal lensing effects. The second DG was used to trigger both lasers and vary the delay time between pulses. All experiments were performed in a single shot manner.

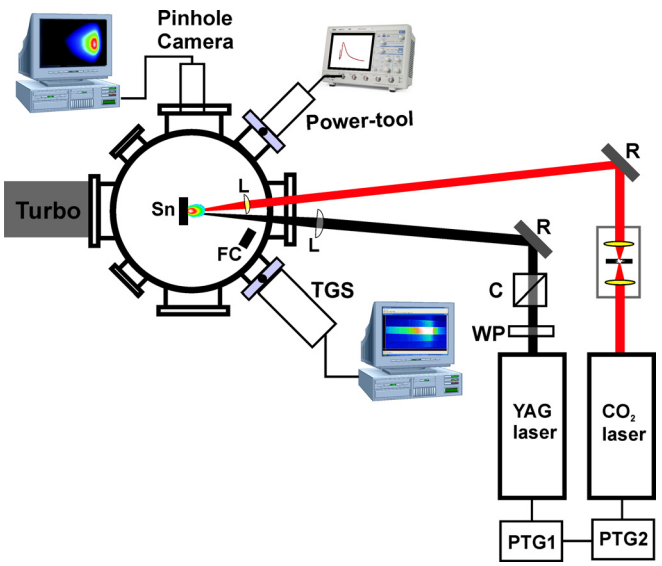

FIG. 1. (Color online) Schematic illustration of the experimental setup. (PTG, delay generator; WP, wave plate; C, cube polarizer; BD, beam dump; R, reflective optics; L, lens; FC, Faraday cup; TGS, transmission grating spectrograph). The Nd:YAG laser generates a pre-plasma that is reheated by the CO_2 laser at a set delay time. Timing generators are used to control triggering of both lasers.

The energy spectra and ion dynamics of the Sn plasma were collected using a FC. The FC was positioned ~ 17 cm from the target at an angle of 15° off-normal and was biased with a -31 V dc voltage. In-band CE is found using an absolutely calibrated EUV power tool. This instrument consists of two 150 nm Zr filters, a Mo/Si mirror, and an EUV photodiode, which collects light at 13.5 nm within a 2% bandwidth. The EUV CE is integrated over a 2π sr solid angle. Data from the FC and EUV power tool are collected and stored using a 1 GHz digital oscilloscope.

The EUV light spectrum emitted from the plasma was captured using an EUV transmission grating spectrograph (TGS) with a silicon nitride 10 000 lines/mm grating, connected to a back-illuminated charge coupled device (CCD). Images of the emission region were captured using a pinhole camera coupled

to x-ray CCD. The pinhole camera used a Zr filter with 50 μm pinhole to capture emission in the 7-15 nm EUV region at 11.5 $\times$ magnification.

III. RESULTS AND DISCUSSION

Our previous studies[3,11] have shown that the optimum laser pulse parameter for obtaining the highest CE for a CO_2 laser was 6×10^9 W/cm^2 with a spot size of 225 μm. Therefore, we used this laser intensity for the present study. At this laser intensity[3] the measured peak density of the CO_2 LPP was estimated to be 5.5×10^{19}/cm^3, which is higher than the critical density of a CO_2 LPP (9.8×10^{18}/cm^3). Once this critical density is reached, the long laser pulse can no longer penetrate through the plasma and ablate more of the target. The laser radiation will instead be used to further heat the expanding coronal region, increasing photon emission. Due to the higher critical density for a Nd:YAG LPP (9.8×10^{20}/cm^3) and a shorter laser pulse duration, laser radiation will be absorbed mainly near the target surface. An increased plasma density can result in higher self-absorption of EUV photons emitted by the plasma and a lower CE.

When evaluating which laser should be used for the prepulse and the pumping pulse, we see that due the two orders of magnitude difference in critical densities, if a CO_2 laser were used for the prepulse and a Nd:YAG laser for the pumping pulse, at peak pre-plasma density, the pumping pulse would still be able to penetrate through the less-dense pre-plasma and interact with the target, rather than reheat the pre-plasma. This would result in denser plasma, exhibiting stronger self-absorption and lower CE. If the Nd:YAG laser is used for the prepulse and the CO_2 laser for the pumping pulse, the pre-plasma will be opaque to the pumping pulse and laser radiation will be used to more efficiently reheat the coronal region of the plasma. This could increase EUV photon emission in a less-dense region, thereby limiting self-absorption. This irradiation scheme provides the optimum EUV emission parameters, resulting in enhanced conversion efficiency.

CO_2 laser pulse energy of 110 mJ, with a power density of 6×10^9 W/cm^2, was used throughout the experiment. Energies from the Nd:YAG laser were 15, 25, and 50 mJ and were adjusted using a combination of wave plate and cube polarizer. Both lasers were focused onto a planar Sn target. The EUV emission spectra from the CO_2 laser and Nd:YAG laser at varying intensities were recorded and can be seen in Fig. 2. The laser spot sizes used in obtaining this data were 100 μm and 225 μm for the Nd:YAG and CO_2 lasers, respectively. The Sn UTA emission given in Fig. 2 is the result of excited Sn ions ranging from Sn^{8+} to Sn^{13+}, with the lower charged ions emitting at higher wavelengths. The comparison between Nd:YAG and CO_2 LPP emission shows higher spectral purity exhibited by the CO_2 LPP centered at 13.5 nm. The dip in the Nd:YAG spectra near 13.5 nm can be explained by the reabsorption in the plasma.[29] The Nd:YAG LPP emits a broader UTA, especially in the higher wavelength side, due to an enhanced rate of three-body recombination arising from its higher electron density.[16]

With a chosen irradiation scheme for the prepulse, additional parameters needed to be investigated to obtain an optimum EUV conversion efficiency. The parameters studied include the delay time between prepulse and pumping pulse and the laser intensity of the prepulse. The delay between pulses allows for sufficient expansion of the pre-plasma for coupling with the pumping pulse. By varying the prepulse laser intensity, the pre-plasma density, ion energies, and plasma expansion rates will change. Fig. 3 shows the results of varying the delay time between prepulse and pumping pulse. Prepulse intensities used were 3.2×10^{10} W/cm^2, 5.3×10^{10} W/cm^2, and 1.1×10^{11} W/cm^2, corresponding to 15 mJ, 25 mJ, and 50 mJ laser energies, respectively. Pumping pulse intensity remained constant at 6.0×10^9 W/cm^2 and provided an individual CE of 2.3%. Delay times found in the figure highlight only those regions where the peak CE was obtained. An extended delay time range up to 2 μs was

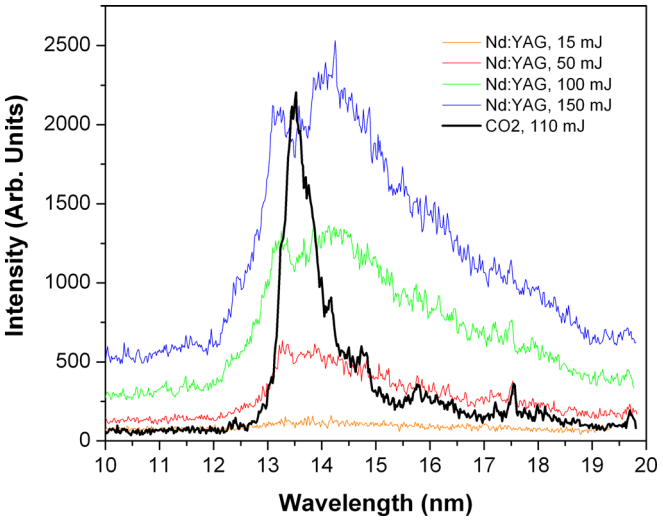

FIG. 2. (Color online) EUV spectra of individual pulse CO_2 and Nd:YAG LPP emission at varying laser energies. Nd:YAG plasmas generate broad EUV emission, while CO_2 plasmas exhibit high spectral purity centered near 13.5 nm.

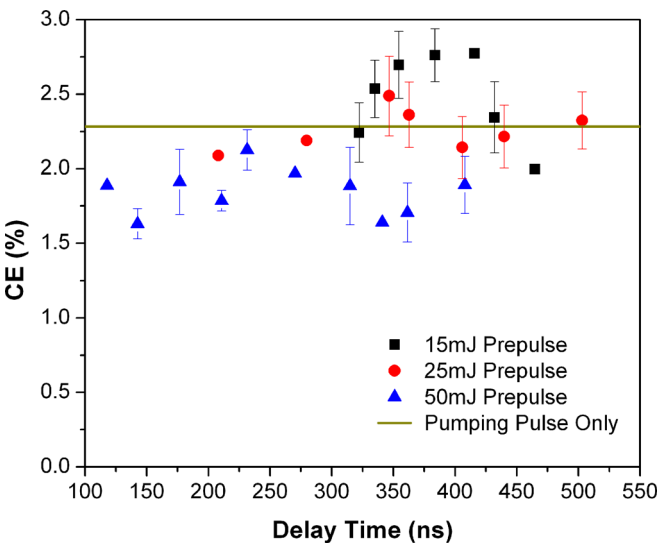

FIG. 3. (Color online) EUV CE with varying delay time between laser pulses and varying prepulse laser intensities. CE was calculated using energies of both prepulse and pumping pulse. Prepulse laser spot size was 100 μm, and pumping pulse spot size was 225 μm. Maximum CE enhancement in this calculation of CE was ~25%.

TABLE I. EUV CE comparison for varying prepulse energy and spot size.

	Prepulse energy (mJ)	Peak delay time (ns)	CE improvement (including prepulse energy)	CE improvement (excluding prepulse energy)
100 μm	15	390	23%	41%
spot size	25	340	12%	36%
	50	225	−6%	39%
250 μm	15	575	3%	17%
spot size	25	550	−8%	14%
	50	400	−19%	19%

also investigated, but showed no significant results and is not presented here. It was found that increasing the prepulse intensity shifted the peak CE to earlier delay times. This was caused by faster expansion of the prepulse plume with higher prepulse laser intensity, resulting in a lower delay time needed to obtain optimum pre-plasma conditions for the pumping pulse. This data were also repeated using the same prepulse and pumping pulse energies but by changing the prepulse spot size to 250 μm, thereby reducing prepulse intensities almost one order of magnitude. Results and trends were consistent with those from Fig. 3 and can be seen in Table I, but peak delay times were longer due to slower preplasma expansion from lower prepulse intensities.

Note that CE decreased substantially as prepulse energy was increased. This is because the CE was calculated as a function of the combined laser energy from the prepulse and pumping pulse. By excluding the prepulse energy when calculating the efficiency, the CE did not increase proportionally with increasing prepulse energy, as seen in Table I. Instead, CE was found to remain constant at nearly 40% improvement compared to emission from the pumping pulse alone. By including prepulse energy in the CE calculation, peak CE was found to increase almost 23% with the lowest prepulse energy. By changing the prepulse spot size to 250 μm, thereby reducing prepulse intensities, the CE decreased significantly. Maximum CE increases were 15%, excluding prepulse energy, for all prepulse energies and only peaked at 3% for the lowest energy prepulse when including prepulse energy.

Fig. 4 shows how the prepulse energy affects the peak delay time at which maximum CE is observed. As seen in the figure, the peak delay time follows a linear trend with increasing prepulse energy at a fixed prepulse spot size. This relation can be useful for predicting the peak delay when evaluating different prepulse parameters. From these results we conclude that a balance of high prepulse intensity and low prepulse energy relative to pumping pulse energy provide best CE enhancements. The high prepulse intensity creates a more dense initial plasma, while low prepulse energy relative to the pumping pulse assures that the CE will not be significantly decreased by the increase in the total laser energy.

EUV emission spectra using a prepulse at the optimum intensity for maximizing CE and at the peak delay between pulses is shown in Fig. 5 and compared to the emission spectra of the individual prepulse and pumping pulse. Peak intensities throughout the 13.5 nm in-band region were

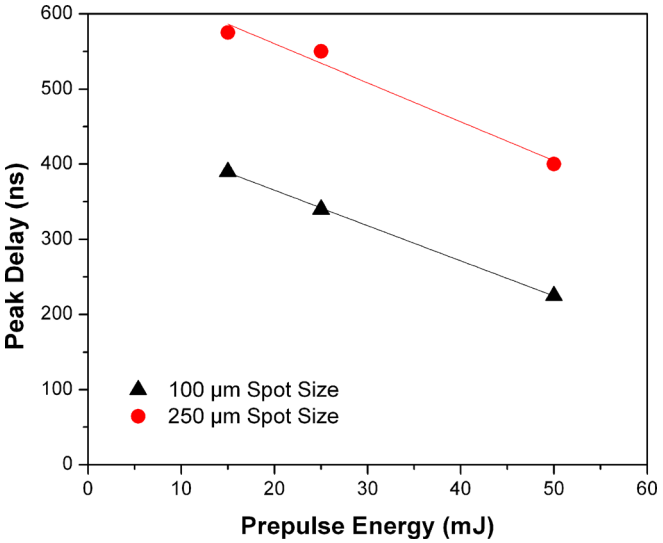

FIG. 4. (Color online) Relation for peak delay between laser pulses and prepulse energy at a fixed prepulse spot size was found to be linear and exhibit near identical curve-fit slopes.

increased using a prepulse, compared to the emission intensities for the pumping pulse alone. However, increased intensities of out-of-band radiation indicate worsening spectral purity. As seen in the figure, it is evident that the prepulse alone produced negligible EUV emission. Therefore, it is certain to conclude that the increased emission intensities seen using a prepulse were generated by the interaction of the pumping pulse with the pre-plasma and not from the preplasma's own emission.

Fig. 6 shows the ion yield for the prepulse system at the optimum prepulse intensity for maximizing CE and at the peak delay between the two pulses and is compared to the ion yields for the individual prepulse and pumping pulse. The "Zero" time shown for the prepulse system data corresponds to the start of the prepulse. Data recorded for the individual prepulse and pumping pulse has been shifted and

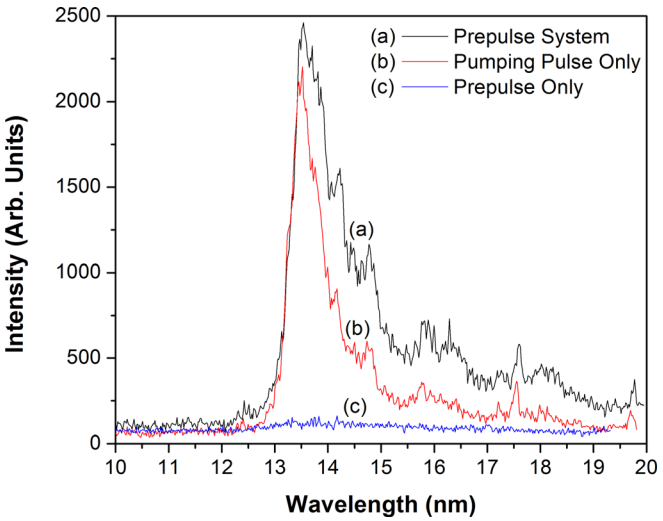

FIG. 5. (Color online) EUV emission spectra indicating a broadening of the spectrum for a reheated plasma. The prepulse only spectrum used a 15 mJ Nd:YAG pulse, the pumping pulse only spectrum used a 110 mJ CO_2 pulse, and the prepulse scheme spectrum used a 15 mJ prepulse, and 110 mJ pumping pulse with a 390 ns delay.

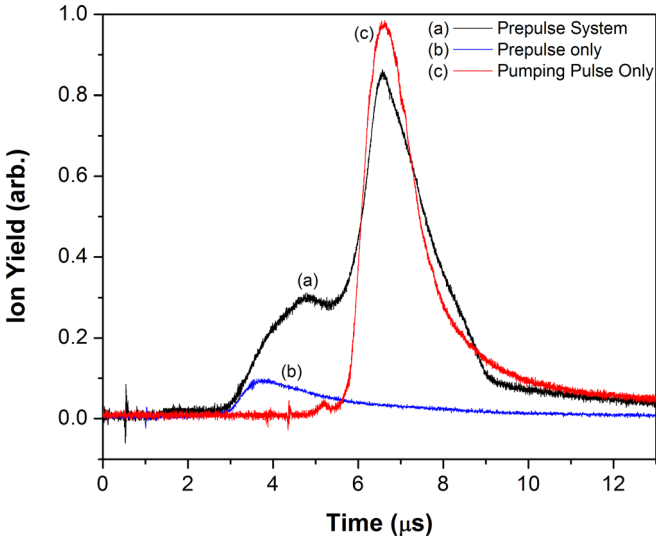

FIG. 6. (Color online) Ion yields collected from Faraday cup indicating a portion of pumping pulse energy being absorbed by the pre-plasma. Prepulse only and pumping pulse only data has been shifted along to time scale to correspond with related features from the prepulse scheme for comparison purposes. "Zero" time for prepulse scheme data corresponds to the start of the prepulse. The prepulse only data used a 15 mJ Nd:YAG pulse, the pumping pulse only data used a 110 mJ CO_2 pulse, and the prepulse scheme data used a 15 mJ prepulse, and 110 mJ pumping pulse with a 390 ns delay.

aligned with the corresponding features from the prepulse system data for comparison purposes. The first spike in the prepulse system, peaking near 4.5 μs, represents the ions from the pre-plasma that were further excited by the pumping pulse. The increased ion yield of this peak compared to the yield of the prepulse alone is mainly caused by the ionization of atomic particles in the pre-plasma by the pumping pulse. The second spike in the prepulse system, peaking near 6.5 μs, represents the pumping pulse interacting with the planar target. The existence of the second spike indicates that only a portion of the pumping pulse is used to heat the pre-plasma. Because pulse length of the prepulse is only about 15% of the pumping pulse, sufficient pre-plasma densities for reheating are only existent for a portion of the pumping pulse. This means that once the pre-plasma density drops below the critical density of the CO_2 plasma, the pumping pulse will penetrate the pre-plasma and begin ablating directly from the target, rather than reheating the pre-plasma. If the initial plasma density from the prepulse exceeds the critical density of the pumping pulse and was able to be maintained throughout the duration of the pumping pulse, further enhancements of EUV emission may be possible.

EUV pinhole camera images can be seen in Fig. 7. These images represent EUV light emission from each LPP configuration. Negligible emission from the prepulse image supports the conclusion from Fig. 5 that the prepulse emission intensity is not the cause of increased intensity found in the prepulse system emission. By comparing the image of the pumping pulse only with the prepulse system image, it can be seen that the size of the emitting plasma is slightly increased and the intensity of EUV light is increased with the use of a prepulse, representing increased EUV emission and therefore higher CE.

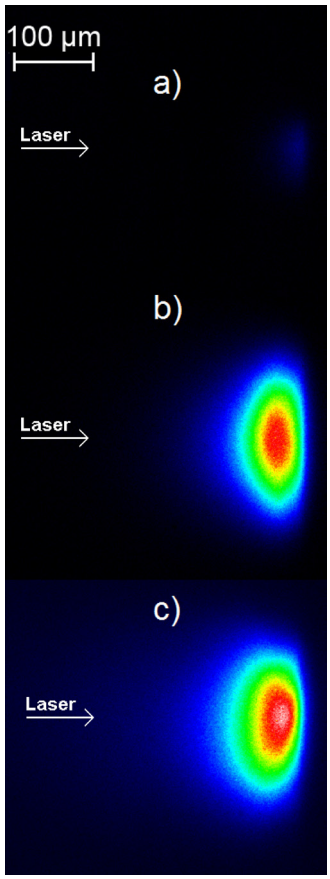

FIG. 7. (Color online) Pinhole camera images showing EUV emission from plasmas of (a) the 15 mJ Nd:YAG prepulse, (b) the 110 mJ CO2 pumping pulse, and (c) the prepulse scheme using a 15 mJ prepulse and 110 mJ pumping pulse with a 390 ns delay. Source size and intensity were improved using the prepulse scheme.

We obtained a maximum of 40% enhancement in EUV emission from the reheated plasma, though previous modeling results have shown substantially higher values.[12] Much recent modeling has been performed using spherical target geometries.[4] The expansion and, hence, density profiles of plasmas from planar and spherical targets differ greatly.[4] Planar target plasma expansion tends to be cylindrical in form, resulting in a steep density gradient and lower lateral expansion. Efficient coupling between prepulse plasma and the pumping pulse, with a large spot size compared to that of the prepulse, may require longer delay times due to slower lateral expansion, at which point plasma densities may be significantly reduced. For spherical targets, plasma expansion is more spherical, with a smoother density profile. This results in faster lateral expansion, so a shorter delay between pulses will be necessary and a higher plasma density may be attained. This could be an ideal condition for a CO_2 laser pumping pulse, since the initial higher density plasma will produce more efficient reheating of the plasma therefore, enhancing EUV emission.

IV. CONCLUSION

We investigated the effects of prepulses for enhancing EUV emission from a Sn LPP. It was decided from plasma density and critical laser density data that Nd:YAG laser operating at 1.06 μm should be used for prepulses and CO_2

laser at 10.6 μm should serve as the pumping pulses for generating EUV emission. Parameters studied to optimizing EUV emission were laser intensity of the prepulse to generate a dense enough initial plasma and the delay time between prepulses and pumping pulses to allow for the initial plasma expansion before reheating by the pumping pulse. We found that by balancing prepulse laser intensity and energy, improvements of up to 40% in CE were found with varying prepulse energies when excluding the prepulse energy from the efficiency calculation. When including the prepulse energy in the calculations, improvements of about 25% in CE were seen using the lowest prepulse energies. These improvements are caused by the interaction of the pumping pulse with the opaque initial plasma, generated by the prepulse causing reheating of the coronal region of this initial plasma and creating conditions for higher EUV emission and low self-absorption. These conditions resulted in overall improved net EUV emission and conversion efficiency.

By reheating the initial plasma from prepulses, higher intensities and a broadening of the EUV emission spectrum were obtained by efficiently exciting more ionic transitions in the Sn UTA. Ion yield data showed that only a portion of the pumping pulse was able to interact with the initial prepulse plasma before the plasma density decreased beyond the threshold of the pumping pulse critical density. Once this occurred, the pumping pulse began ablating the target instead of reheating the prepulse initial plasma. If high prepulse initial plasma densities above the critical density of the pumping pulse were to be maintained throughout the pumping pulse duration, EUV emission could be further increased. This may be achieved through the use of spatial confinement of the initial prepulse plasma, spherical targets, and a prepulse with longer duration.

ACKNOWLEDGMENTS

This work is partially supported by the College of Engineering, Purdue University and SEMATECH Corporation.

[1]J. S. Taylor and R. Soufli, in *EUV Lithography*, edited by V. Bakshi (SPIE and John Wiley & Sons, Inc., Bellingham, WA/Hoboken, NJ, 2009), p. 188.
[2]V. Y. Banine, K. N. Koshelev, and G. H. P. M. Swinkels, J. Phys. D **44**, 253001 (2011).
[3]S. S. Harilal, T. Sizyuk, A. Hassanein, D. Campos, P. Hough, and V. Sizyuk, J. Appl. Phys. **109**, 063306 (2011).
[4]A. Hassanein, T. Sizyuk, V. Sizyuk, and S. S. Harilal, J. Micro/Nanolith. MEMS MOEMS **10**(3), 033002 (2011).
[5]V. Bakshi, in *EUV Sources for Lithography*, edited by V. Bakshi (SPIE – The International Society for Optical Engineering, Bellingham, WA, 2006).
[6]U. Stamm, J. Kleinschmidt, K. Gäbel, G. Hergenhan, G. Schriever, and C. Ziener, in paper presented at the EUV Source Workshop on EUV Source Development at XTREME Technologies: An Update, San Jose, CA, 27 February 2005 (SEMATECH Inc., EUV Source Workshop).
[7]N. Ueda, M. Nagata, H. Nishimura, S. Fujioka, T. Aota, Y. Yasuda, Y. Inubushi, T. Ando, T. Norimatsu, M. Nakai, K. Nagai, K. Nishihara, A. Sunahara, N. Miyanaga, Y. Izawa, and K. Mima, Jap. J. Appl. Phys. **45**, 5951 (2006).
[8]H. Mizoguchi, A. Endo, T. Ariga, T. Miura, H. Hoshino, Y. Ueno, M. Nakano, H. Komori, A. Sumitani, T. Abe, T. Suganuma, G. Soumagne, H. Someya, Y. Takabayashi, and K. Toyoda, Proc. SPIE **6151**, 61510S (2006).
[9]J. Pankert, in papter presented at EUV Source on Philips's EUV Source: Update and Issues, San Jose, CA, 27 February 2005 (SEMATECH Inc., EUV Source Workshop).
[10]J. White, P. Dunne, P. Hayden, F. O'Reilly, and G. O'Sullivan, Appl. Phys. Lett. **90**, 181502 (2007).
[11]S. S. Harilal, T. Sizyuk, V. Sizyuk, and A. Hassanein, Appl. Phys. Lett. **96**, 111503 (2010).
[12]K. Nishihara, A. Sunahara, A. Sasaki, S. Fujioka, Y. Shimada, M. Nunami, H. Tanuma, M. Murakami, T. Aota, K. Fujima, H. Furukawa, T. Nishikawa, F. Koike, R. More, T. Kato, V. Zhakhovskii, K. Gamata, F. Ueda, H. Nishimura, Y. Yuba, K. Nagai, N. Miyanaga, Y. Izawa, and K. Mima, Proc. SPIE **6921**, Y9210 (2008).
[13]V. Sizyuk, A. Hassanein, and V. Bakshi, J. Micro/Nanolith MEMS MOEMS **6**, 043003 (2007).
[14]B. Rollinger, O. Morris, N. Chokani, and R. S. Abhari, Proc. SPIE **7636**, 76363F (2010).
[15]S. Fujioka, H. Nishimura, T. Okuno, Y. Tao, N. Ueda, T. Ando, H. Kurayama, Y. Yasuda, S. Uchida, Y. Shimada, M. Yamaura, Q. Gu, K. Nagai, T. Norimatsu, H. Furukawa, A. Sunahara, Y. Kang, M. Murakami, K. Nishihara, N. Miyanaga, and Y. Izawa, Proc. SPIE **5751**, 578 (2005).
[16]D. Campos, S. S. Harilal, and A. Hassanein, J. Appl. Phys. **108**, 113305 (2010).
[17]S. S. Harilal, M. S. Tillack, Y. Tao, B. O'Shay, R. Paguio, and A. Nikroo, Opt. Lett. **31**, 1549 (2006).
[18]S. Fujioka, M. Shimomura, Y. Shimada, S. Maeda, H. Sakaguchi, Y. Nakai, T. Aota, H. Nishimura, N. Ozaki, A. Sunahara, K. Nishihara, N. Miyanaga, Y. Izawa, and K. Mima, Appl. Phys. Lett. **92**, 241502 (2008).
[19]H. Mizoguchi, T. Abe, Y. Watanabe, T. Ishihara, T. Ohta, T. Hori, A. Kurosu, H. Komori, K. Kakizaki, A. Sumitani, O. Wakabayashi, H. Nakarai, J. Fujimoto, and A. Endo, Proc. SPIE **7636**, 763608 (2010).
[20]Y. Tao, M. S. Tillack, S. S. Harilal, K. L. Sequoia, and F. Najmabadi, J. Appl. Phys. **101**, 023305 (2007).
[21]R. W. Coons, S. S. Harilal, D. Campos, and A. Hassanein, J. Appl. Phys. **108**, 063306 (2010).
[22]S. S. Harilal, R. W. Coons, P. Hough, and A. Hassanein, Appl. Phys. Lett. **95**, 221501 (2009).
[23]H. Tanaka, A. Matsumoto, K. Akinaga, A. Takahashi, and T. Okada, Appl. Phys. Lett. **87**, 041503 (2005).
[24]A. Takahashi, D. Nakamura, K. Tamaru, T. Akiyama, and T. Okada, Appl. Phys. B **92**, 73 (2008).
[25]D. Campos, S. S. Harilal, and A. Hassanein, Appl. Phys. Lett. **96**, 151501 (2010).
[26]T. Higashiguchi, K. Kawasaki, W. Sasaki, and S. Kubodera, Appl. Phys. Lett. **88**, 161502 (2006).
[27]M. Anand, S. Kahaly, G. Kumar, M. Sandhu, and P. Gibbon, Appl. Phys. Lett. **88**, 18111 (2006).
[28]N. Hurst and S. S. Harilal, Rev. Sci. Instrum. **80**, 035101 (2009).
[29]Y. Tao, S. S. Harilal, M. S. Tillack, B. O'Shay, and F. Najmabadi, Opt. Lett. **31**, 2492 (2006).